Optical Single-Photon Detection in Micrometer-Scale NbN Bridges

Yu. P. Korneeva[*]
Physics Department, Moscow State University of Education, Moscow 119991, Russia

D. Yu. Vodolazov
Institute for Physics of Microstructures, Russian Academy of Sciences,
Nizhny Novgorod 603950, GSP-105, Russia
and Physics Department, Moscow State University of Education, Moscow 119991, Russia

A. V. Semenov
Physics Department, Moscow State University of Education, Moscow 119991, Russia
and Moscow Institute of Physics and Technology (State University), Moscow 141700, Russia

I. N. Florya and N. Simonov
Physics Department, Moscow State University of Education, Moscow 119991, Russia

E. Baeva
Higher School of Economics National Research University, Moscow 101000, Russia
and Physics Department, Moscow State University of Education, Moscow 119991, Russia

A. A. Korneev
Physics Department, Moscow State University of Education, Moscow 119991, Russia;
Moscow Institute of Physics and Technology (State University), Moscow 141700, Russia;
and Higher School of Economics National Research University, Moscow 101000, Russia

G. N. Goltsman
Physics Department, Moscow State University of Education, Moscow 119991, Russia
and Higher School of Economics, National Research University, Moscow 101000, Russia

T. M. Klapwijk
Physics Department, Moscow State University of Education, Moscow 119991, Russia
and Kavli Institute of Nanoscience, Delft University of Technology, Delft 2628 CJ, The Netherlands

(Received 2 February 2018; revised manuscript received 16 May 2018; published 22 June 2018)

We demonstrate experimentally that single-photon detection can be achieved in micrometer-wide NbN bridges, with widths ranging from 0.53 to 5.15 μm and for photon wavelengths of 408 to 1550 nm. The microbridges are biased with a dc current close to the experimental critical current, which is estimated to be about 50% of the theoretically expected depairing current. These results offer an alternative to the standard superconducting single-photon detectors, based on nanometer-scale nanowires implemented in a long meandering structure. The results are consistent with improved theoretical modeling based on the theory of nonequilibrium superconductivity, including the vortex-assisted mechanism of initial dissipation.

DOI: 10.1103/PhysRevApplied.9.064037

I. INTRODUCTION

The present superconducting nanowire single-photon detectors (SSPDs) are based on long meandering superconducting strips with a width in the range of 50 to 150 nm [1]. It has been empirically found that the use of wider strips leads either to the loss of the single-photon nature of the response or to a rather small detection efficiency [2,3]. This result is in line with the initial interpretation of this type of detector [4,5], in which it was understood that the width of the supercurrent-carrying strip should be comparable to the diameter, D, of the normal hot spot (a region where the superconducting state is suppressed) due to the absorption of the photon. If the strip is biased near its experimentally determined critical current, the emergence of the hot spot forces a redistribution of the supercurrent,

---

[*] korneeva@rplab.ru

leading to a locally enhanced supercurrent density, triggering the switch to the resistive state. Using simple estimates based on the conservation of energy and typical parameters for niobium nitride (NbN), given the energy of an optical photon, leads to $D \sim 40$ nm for the expected size of the normal hot spot [6].

This geometrical mechanism to exceed the critical current density has initiated a more thorough analysis of the conditions of the superconducting strips under current bias by Zotova and Vodolazov [7,8]. They consider a superconducting strip, biased sufficiently close to the intrinsic *depairing* current I_{dep}. Then a small amount of energy can switch the current-carrying superconductor to a resistive state, with the needed energy going to zero when I approaches I_{dep}. The only requirement for the width of the strip is that it should be smaller than the Pearl penetration depth $\Lambda = 2\lambda^2/d$ (with λ being the London penetration depth for a dirty superconductor and d the thickness of the strip). Under these conditions, the supercurrent is uniform across the width, whereas for wider strips the supercurrent is distributed nonuniformly. For a typical NbN film with a thickness of about 5 nm and $\lambda \sim 470$ nm [9], one obtains $\Lambda \simeq 90$ μm.

Using the microscopic theory for superconductivity, it was shown in Refs. [7,8] that, if such a strip with a uniform supercurrent I can be biased at $I \gtrsim 0.5–0.7 I_{\mathrm{dep}}$, the superconducting state becomes unstable in response to relatively small additions of energy in the form of a localized disturbance, loosely called a “hot spot.” Its specific nature in terms of the microscopic theory of nonequilibrium superconductivity has not yet been worked out. It is considered to be a localized nonequilibrium distribution over the energies and with at least a depressed local energy gap initially surrounded by an equilibrium superconductor. The dynamics of such an “impact crater” in the superconducting film depends on the materials.

In previous work, this process was mostly described by what we label as a “geometric-hot-spot model.” The essential feature of this approach is that the supercurrent, initially carried over the full width w of the supercurrent in the wire, is pushed to a more narrow part, excluding the “hot” part with a diameter d. This increased current density then may exceed the critical current density initiating a transition to a voltage-carrying state. To optimize the efficiency of detection, the wire should be on the order of the size d of the hot spot in the superconductor created by the absorbed photon. This geometric-hot-spot model is often used for qualitative discussions and has, for the most part, been leading technological development.

More recently, the microscopic approach has emerged, including the use of nonequilibrium superconductivity. In this approach, the phase coherence of the superfluid flow is fully taken into account, as well as the emergence of resistivity in the superconductor by the creation of vortices. In order to make a clear distinction with previous approaches, we call this the “photon-generated superconducting vortex model.” The theory states that the efficiency of the photon detection is not determined by the geometry, as long as the initial current density is uniform and close to the critical pair-breaking current. The requirement for uniformity of the current density was given previously. If the superconducting wire can be biased close to the critical pair-breaking current, all photons can be detected, wherever they hit the wire, because all of them create a sufficient disturbance to trigger a *local* excess of the critical current density, initiating the creation of vortex-antivortex pairs. In the film, vortex-antivortex pairs are created inside the hot spot (if it is located far from the edge of the strip) or by vortex entry into the strip (if the hot spot is located close to the edge). The motion of a vortex and/or antivortex due to the Lorentz force leads to a voltage in the superconductor and, eventually, to the appearance of a normal domain [8]. Rather than assuming a fully normal hot spot, this model takes into account the resistive properties of the superconducting state due to vortex movement, with details determining the full dynamics.

In order to build experimentally on a model based on current densities close to the critical pair-breaking current, one needs to determine whether the observed critical current is determined by intrinsic or extrinsic properties, such as material imperfections. The commonly used material for single-photon detection is NbN with a thickness of about 5 nm, chosen because of its fast electron-phonon relaxation, including phonon escape to the substrate. However, such films have a fairly high resistivity, a low diffusion constant, and a high resistance per square on the order of 800 Ω, which implies that they have an intrinsic tendency to become electronically inhomogeneous with a spatially fluctuating superconducting energy gap [10,11], which may worsen due to material imperfections. Therefore, it is to be expected that the critical current for a long superconducting wire is determined by the weakest spot, which statistically will be the lowest value of the energy gap along the wire. Second, in order to know the value of the critical depairing current, one has to rely on a quantitative estimate based on measured parameters, and preferably on a comparison with the functional dependence, such as that carried out for aluminum by Romijn *et al.* [12]. Relatively high critical current densities were reported recently by Charaev *et al.* [13], although in more narrow strips, larger values have been reported [3,14]. Nevertheless, the maximally reachable value is not known and, given the expected inhomogeneities, may vary. Instead, we decide to work with relatively short microbridges and vary the width, to minimize the risks of hitting a critical current that is too low while expecting a reasonably uniform current density.

In this work, we report on our findings, that relatively wide NbN bridges with widths in the range of 0.53 to 5.15 μm are able to detect single photons of wavelengths ranging from 408 to 1550 nm. We determine the internal detection efficiency, η, the detection efficiency normalized to the absorption, for different bias currents I and find that it reaches a value in the tens of percent near the experimental critical current I_c. From the experimental data, we distinguish between two regimes. Regime I, in which a sharp increase in η is observed for an increasing current, is analogous to the conventional meanderlike SSPDs. It is followed by a much slower increase of the η upon approaching I_c, which we label regime II. We attribute regime I to fluctuation-assisted photon detection with the slope of the η as a function of current I comparable to the slope of the number of dark counts with the bias current. We attribute regime II to deterministic photon counting, as described theoretically by Zotova and Vodolazov [15]. We are able to explain quantitatively the dependence of the η on the current I in regime II for the short wavelengths, taking into account the actual geometry of our samples. We argue that, in this parameter range, we observe an η close to unity.

Our findings offer an alternative route towards superconducting single-photon detectors with a short dead time, a few hundred picoseconds, because of the relatively small kinetic inductance of short superconducting bridges in comparison to the conventional superconducting meanders [1]. Additionally, our results provide support for the relevance of the vortex-assisted contribution to photon detection, as proposed by one of the authors [8].

II. SAMPLES AND CHARACTERIZATION

Our samples are planar constriction-type microbridges, as shown in Fig. 1. They are made from reactively sputtered NbN films with a thickness 5.8 nm, determined from a calibrated sputter rate and a sputter time. The width w of the bridges at the narrowest point varies from 0.53 to 5.15 μm. The constriction-type topology is chosen to prevent current crowding effects [16] and to maximize the chance to reach in the experiments the critical pair-breaking current. Note that, given the properties of the NbN films, the constrictions are much larger in length and width than the coherence length. Therefore, it is assumed that the wider part with the lower current density does not lead to an enhancement of the critical pair-breaking current, in contrast to the case treated by Aslamazov and Larkin [17], because of the short coherence length in NbN [18]. The parameters of the studied devices are summarized in Table I. The details of the fabrication process are presented in Appendix A.

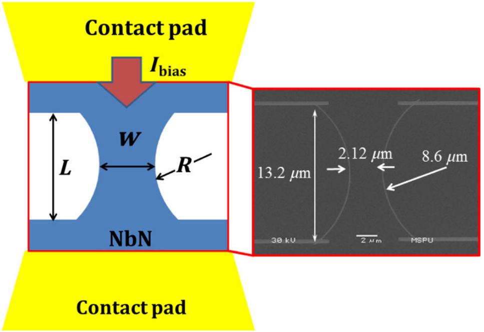

FIG. 1. Drawing of a typical NbN constriction-type bridge with a scanning-electron-microscope (SEM) image of one of the bridges with indicated dimensions (sample C in Table I). The contacts on top of the NbN film are made of gold (Au). All bridges have edges designed as a segment of a circle with the radius 8.6 μm.

We experimentally observed critical current densities j_c for two different temperatures $T = 4.2$ K and $T = 1.7$ K. In Table I, these results are listed for a temperature $T = 4.2$ K. Obviously, there is some scatter in the values of the critical temperature, as well as in the critical current density. It indicates that there is some uncontrolled variation from sample to sample, although the samples are from the same film. This variation may be caused by the metallurgy resulting from the deposition conditions, but it may also be intrinsic due to the competition between localization in this low-diffusivity material and superconductivity. For a material like NbN, the experimental values in this experimental geometry are reassuringly close to the

TABLE I. Parameters of the studied samples for a temperature $T = 4.2$ K. The width of the bridge w is at the neck, T_c is the critical temperature determined from the midpoint of the resistive transition, ρ (20 K) is the resistivity at $T = 20$ K, j_c and $j_c^{\rm sh}$ are the critical current densities measured without and with a shunt resistor, and $j_{\rm dep}$ is the calculated depairing current at the indicated temperature, using $j_{\rm dep}$ (0) as the calculated critical depairing current at $T = 0$ following from Eq. (2). The variations in the calculated values are due to the variations in resistance per square determined for each sample. The diffusion constant D is kept constant.

Sample ID	Width (μm)	T_c (K)	ρ (20 K) ($\mu\Omega$ cm)	j_c (4.2 K) (A/cm^2)	$j_c^{\rm sh}$ (4.2 K) (A/cm^2)	$j_{\rm dep}$ (4.2 K) (A/cm^2)	$j_{\rm dep}$ (0) (A/cm^2)
A	0.53	8.25	386	3.16×10^6	3.67×10^6	3.79×10^6	5.94×10^6
B	1.61	8.35	396	2.74×10^6	3.72×10^6	3.81×10^6	5.89×10^6
C	2.12	8.5	393	3.75×10^6	4.43×10^6	4.02×10^6	6.11×10^6
D	3.07	8.35	398	3.06×10^6	3.66×10^6	3.79×10^6	5.87×10^6
E	4.04	8.35	402	2.52×10^6	3.16×10^6	3.75×10^6	5.8×10^6
F	5.15	8.35	427	2.28×10^6	2.57×10^6	3.54×10^6	5.47×10^6

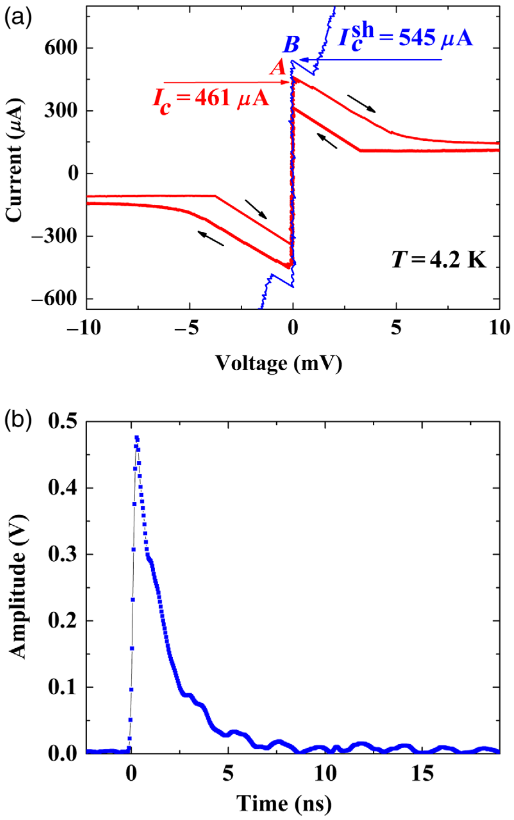

FIG. 2. (a) *I*-*V* curves of sample *C* measured with a 3-Ω shunt resistor (blue) and without one (red) at a temperature $T = 4.2$ K. (b) Single-shot waveform transient from sample *C* when a photon is absorbed.

theoretical values. Since these relatively wide samples have impractically high critical currents, we connect a 3-Ω shunt resistor in parallel to the sample to prevent latching and to enable a spontaneous return to the superconducting state. Although not expected, this connection of the shunt resistor leads to different increases of experimentally observed critical currents. In Fig. 2(a), we show current-voltage characteristics for sample *C* without (the red curve) and with the 3-Ω shunt resistor (the blue curve) with different critical currents (points *A* and *B*, respectively). A similar observation was reported on and discussed previously by Brenner *et al.* [19]. In our measurements, this behavior can be attributed, at least in part, to division of the current between the chip with a superconducting bridge and the shunt: the chip with a superconducting bridge also contains normal resistance, on the order of a few tenths of an ohm, because this is a two-point measurement. Of course, the quantity of interest is a supercurrent, i.e., the current flowing through the sample; hence, we use the measured current with the shunt only as a value to plot the data.

We assume that the theoretical depairing currents can be described by the expression derived for clean superconductors by Bardeen [20]. It deviates by less than 3% from the results of the microscopic calculations for dirty superconductors, which have been compared to experiments on aluminum by Romijn *et al.* [12]:

$$I_{\rm dep}(T) = I_{\rm dep}(0)\left[1 - \left(\frac{T}{T_c}\right)^2\right]^{3/2}, \tag{1}$$

with the prefactor $I_{\rm dep}(0)$, calculated from Eq. (31) in Clem and Kogan [21]:

$$I_{\rm dep}(0) = 0.74\frac{w[\Delta(0)]^{3/2}}{eR_s\sqrt{\hbar D}}. \tag{2}$$

Here, $\Delta(0)$ is the superconducting energy gap at 0 K, e is the electron charge, R_s is the resistance per square, and D is the diffusivity. Strictly speaking, Eqs. (1) and (2) are quantitatively valid for moderately dirty superconductors with $k_F l \gg 1$ (k_F is the Fermi wave vector and l is the mean free path for elastic scattering). We also assume the BCS ratio of $\Delta(0)/k_B T_c \approx 1.76$.

In applying these expressions to the present NbN films, we make a conceptual step, which would require a deeper justification and which is currently not available. It is known that the critical temperature T_c varies with the resistance per square, reminiscent of experiments on the superconductor-insulator transition [9,22–25]. It has also been found that the ratio of $\Delta(0)/k_B T_c$ for such films is not a constant but changes with the resistance per square. It is often attributed to the film properties and the substrate surface [26]. Nevertheless, there is compelling evidence that these materials are anomalous in many respects [27]. Given this uncertainty, we make the choice to take the most straightforward input towards Eqs. (1) and (2), and we use the BCS ratio for Δ, and $k_B T_c$ and for $k_F l \approx 3$–5 [23,25,26,28]. For the diffusion constant, we use $D = 0.31\ {\rm cm}^2\,{\rm s}^{-1}$, which is determined from the upper critical field (see additional details on sample *C* in Appendix A). Similarly, we use Eq. (2) together with the temperature dependence expressed in Eq. (1) as a best estimate for the theoretical depairing current. For further study, we select the samples with the highest ratio of $j_c/j_{\rm dep}$ to analyze the photon response.

Since Eqs. (1) and (2) give rather approximate values of the depairing current for our samples under study, and taking into account the increase of the switching current $j_c^{\rm sh}$ due to the shunt resistor, the ratio $j_c^{\rm sh}/j_{\rm dep}$ should be treated as a semiquantitative estimate which samples are closer to $j_{\rm dep}$, and which are farther. Thus, one should not pay much attention to the absolute values of ratio $j_c^{\rm sh}/j_{\rm dep}$: they all seem to be higher than they actually are and are sometimes even higher than $j_{\rm dep}$ (sample *C*).

Biased near the critical current we observe voltage pulses quite similar to those we routinely observe with the usual meander-type SSPDs. Figure 2(b) presents a typical voltage transient of the 2.12-μm-wide bridge. We do not intend to resolve the rising and falling edges of the pulse precisely, and we use rather simple readout electronics with a 1-GHz band. Nevertheless, one can see that the decay time is much shorter than in the meandering SSPDs, but it is still longer than expected from the kinetic inductance L_k of the bridge [29] connected to the 3-Ω shunt resistor. The value of L_k in our samples is in the range of 0.4 to 1.1 nH, giving a characteristic decay time in the subnanosecond range. We attribute this discrepancy to a parasitic inductance of the readout lines and the mounting. As for the rising edge, its timing is well beyond the capabilities of the readout that we use.

III. SINGLE-PHOTON DETECTION

The photon detection is carried out in an experimental setup that is discussed in detail in Appendix B. Figure 3 presents real-time waveform transients taken with a digital oscilloscope. The top blue curve shows the clock pulses from the laser. The red curves are the responses from the sample measured for decreasing power by increasing the optical attenuation. We observe (1) that the amplitude of the photoresponse does not depend on the attenuation, and (2) that the probability of observing a response drops with the increase of optical attenuation.

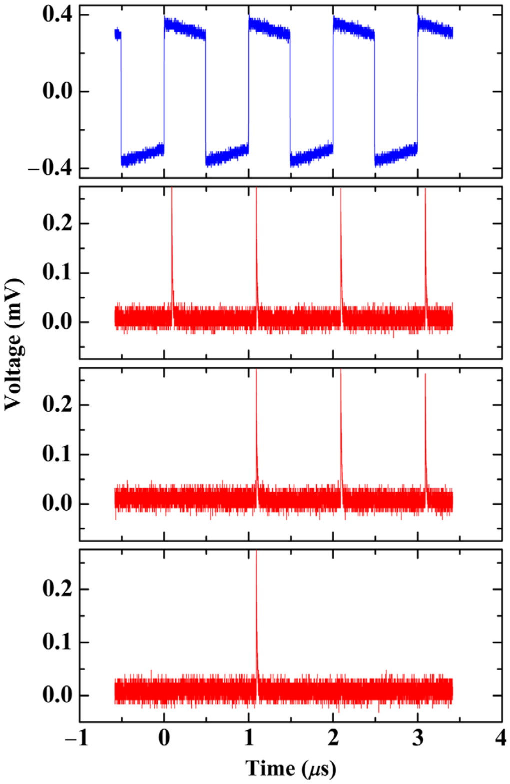

FIG. 3. Real-time waveform record showing clock pulses from the laser (the top blue curve) and photon pulses detected by the bridge at different attenuation levels of the power from the laser (the red curves, with power decreasing from top to bottom). With the increase of attenuation of the power, the number of detected pulses decreases.

We proceed with a statistical analysis of the photon count rate on the number of incident photons used previously in Refs. [30,31]. In the single-photon counting regime, the photon count rate R should be proportional to the photon flux R_{ph}: $R \propto R_{\mathrm{ph}}$. For multiphoton detection, we expect that $R \propto R_{\mathrm{ph}}^n$, with n being the number of simultaneously absorbed photons producing a single count. This behavior follows from the Poisson distribution of the incident photon flux. In a strongly attenuated laser beam, the probability p of having a given number of photons n in a given constant time slot should be distributed according to $p \propto \langle m \rangle \exp(-\langle m \rangle)/n!$, where $\langle m \rangle$ is the mean number of photons in the time slot. The probability p of detecting one photon is proportional to the mean photon number $\langle m \rangle$, the probability of detecting two photons is proportional to $\langle m \rangle^2$, and so on. In Fig. 4, we show the count rate vs the incident photon flux for sample C at three wavelengths—408, 829, and 1550 nm—and for two bias currents. The photon flux is calculated at the input of the fiber, and coupling losses (which are different for different wavelengths) are not taken into account in this plot. We select two bias currents which are supposed to correspond to two different mechanisms of photoresponse, as proposed by Zotova and Vodolazov [15]: (1) regime I (at $I_{\mathrm{bias}} = 0.7I/I_{\mathrm{dep}}$) corresponds to the initial sharp increase of η, and (2) regime II (at $I_{\mathrm{bias}} = 0.9I/I_{\mathrm{dep}}$) denotes a much slower increase of η. More details about these regimes are given below. One can see that, for all studied wavelengths and bias currents, we observe $\propto R_{\mathrm{ph}}$, a dependence which confirms the single-photon operation of the sample. We observe the same results for all studied samples, including the largest, the 5.15-μm-wide sample F.

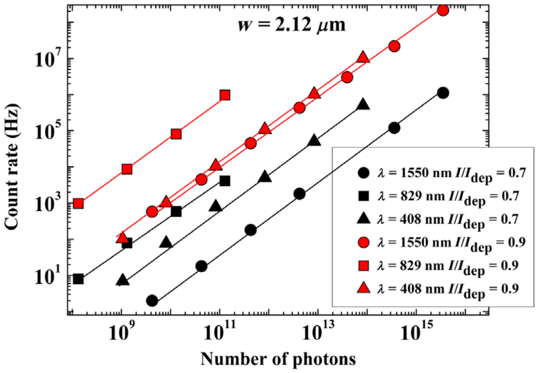

FIG. 4. Count rate versus the number of photons in the laser pulse. Blue symbols are used for $I_{\mathrm{bias}} = 0.7I/I_{\mathrm{dep}}$, red symbols for $I_{\mathrm{bias}} = 0.9I/I_{\mathrm{dep}}$. The linear dependence of the count rate with the number of photons in the pulse corresponds to the Poisson statistics and indicates the single-photon nature of the response, irrespective of the bias current.

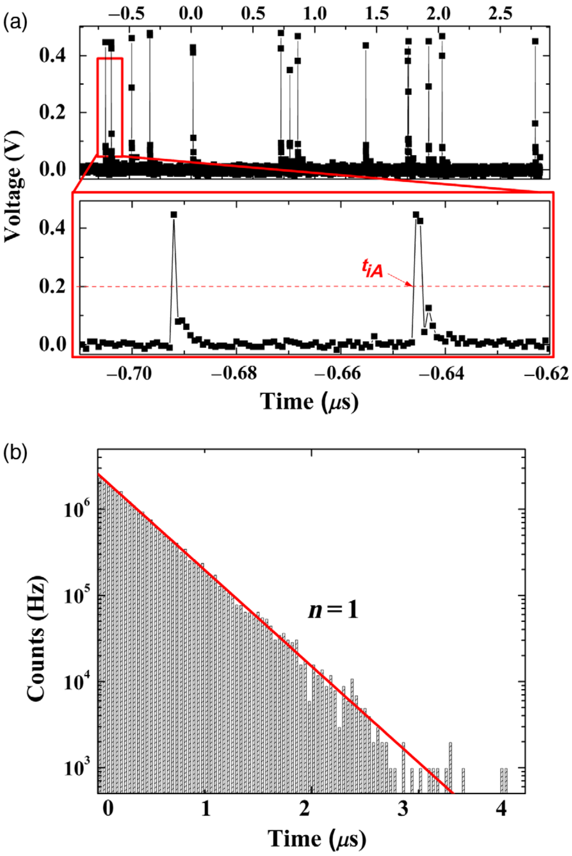

FIG. 5. (a) Oscilloscope waveform transient (top panel) and a fragment of the time trace (bottom panel). (b) Statistical analysis of the interarrival time of the photon counts measured with a cw laser of wavelength $\lambda = 1550$ nm. The exponential distribution of the interarrival time intervals between photon counts shows the same Poisson distribution as the photons in the incoming light, providing additional proof of the single-photon response of the sample.

As a further test of the response, we study the interarrival time distribution of photon counts, as suggested by Marsili *et al.* [32]. The statistics of the interarrival time is studied using the digital oscilloscope Tektronix DPO-70404C. We record the waveform transient of maximum length, which is a total of 12.5×10^6 points, covering 10-ms windows with 800-ps resolution. Such a time resolution makes it possible to obtain at least one point on the rising edge and two to three points on the decreasing edge of the pulse [Fig. 5(a)]. As a result, we have a set of times t_i and, correspondingly, the instantaneous voltages U_i. Then we extract all time moments t_{iA}, which correspond to the appearance of photocounts. As an objective criterion, we take the voltage rise above a threshold value to indicate the voltage pulses U_{iA}, which count as events. U_{iA} is taken to be much larger than the noise amplitude. From the array t_{iA}, we determine the time intervals between all successive photocounts: $\Delta t_i = t_{i+1} - t_i$. From these time intervals we construct a histogram of the distribution of these time intervals, normalized to the number of time intervals and their width. Figure 5(b) shows the histograms of this interarrival time for sample D.

Since the photons in the incoming light from the cw laser are independent and since they obey Poisson statistics, the probability of recording n photons in a time interval t is $(\nu t)^n \exp(-\nu t)/n!$, with ν being the mean photon flux. Let the first count be observed at $t = 0$. The probability of a second count during the interval from t to $t + dt$ is the multiplication of probabilities of having exactly one photon in the interval $[t, t + dt]$, and $n - 1$ photons in $[0, t]$. The probability of the former event is νdt, whereas the latter is $(\nu t)^{n-1} \exp(-\nu t)/(n - 1)!$. Thus, the probability distribution for the second photon count appearance is

$$\rho(t) = \frac{\nu(\nu t)^{n-1} \exp(-\nu t)}{(n-1)!}. \qquad (3)$$

The red straight line in Fig. 5(b) is the prediction of Eq. (3) with $n = 1$ (n is the number of photons for a time interval t). It clearly proves that the sample does not accumulate more than one photon to produce a single photon count.

IV. DEPENDENCE OF DETECTION EFFICIENCY ON CURRENT

In Figs. 6(a) and 6(b), we show the evolution of the η with the bias current. We distinguish between the two regimes indicated in the figure. In regime I, the η grows fast in an exponential-like manner. We associate this regime with fluctuation-assisted photon counting. In this case, the absorption of a photon triggers the transition to the resistive state only with the help of thermally activated vortex nucleation near the point of impact of the photon [15]. The indirect proof of this intrinsic mechanism comes from the fact that the slopes of $\eta(I)$ in regime I and the dependence of the dark count rate on the bias current [see Figs. 6(a) and 6(b)] are identical for all samples and bias conditions.

The second regime, regime II, begins at a current denoted by $I \gtrsim I_2$, which we relate to the position-dependent photon counting proposed in Refs. [8,15,33]. It is worth noting that I_2 is an arbitrarily chosen value at which $\eta = 1\%$. This method gives a reasonable accuracy, as below I_2, η increases sharply with an increasing bias current. In this deterministic regime, the η monotonically grows with the current, starting from the current called $I_{\rm det}^{\rm min}$, where the region near the edges of the sample (with a typical width of about the diameter of the hot spot) starts to detect photons. It grows up to a current $I_{\rm det}^{\rm max}$, at which the central part of the sample joins the detection process. For relatively narrow widths, it is expected that $I_{\rm det}^{\rm min} \simeq I_{\rm det}^{\rm max} - 0.1 I_{\rm dep}$ (see Fig. 9 in Ref. [8]). The calculations for wider samples give $(I_{\rm det}^{\rm max} - I_{\rm det}^{\rm min})/I_{\rm dep}$ in range 0.03–0.04, and the dependence $\eta(I)$ has a steplike form with $\eta \ll 1$ for $I < I_{\rm det}^{\rm min}$ and $\eta = 1$

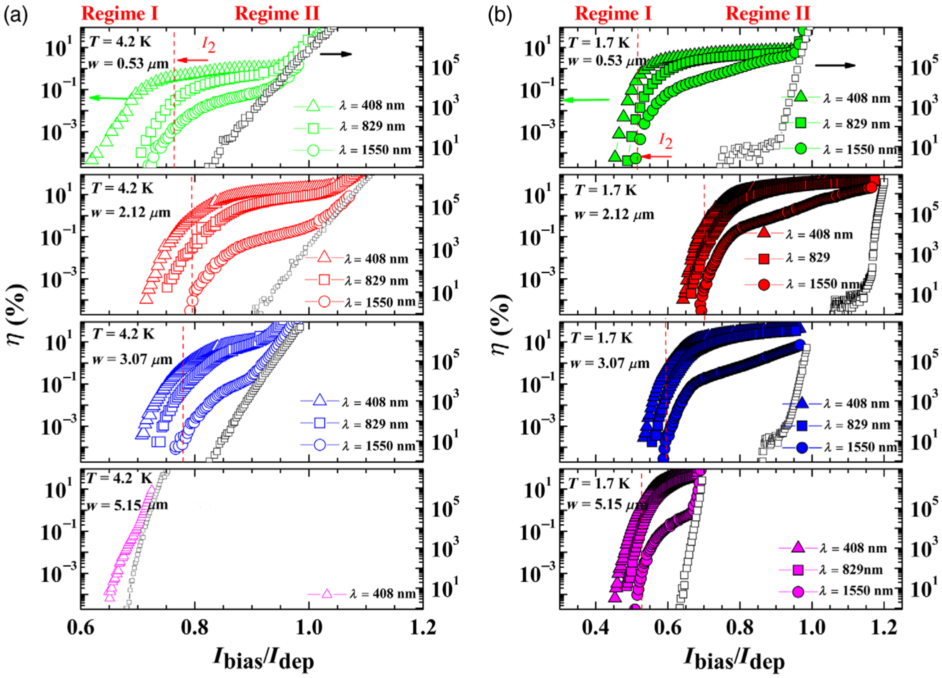

FIG. 6. Dependence of detection efficiency on a bias current normalized to the absorption, $\eta(I)$. The bias current I_{bias} is normalized to the calculated depairing current I_{dep}. (a) η at 4.2 K and (b) η at 1.7 K for samples (from top to bottom) A, with $w = 0,\ 53\ \mu$m (the green symbols); C, with $w = 2,\ 12\ \mu$m (the red symbols); D, with $w = 3,\ 07\ \mu$m (the blue symbols); and F, with $w = 5,\ 15\ \mu$m (the magenta symbols). These dependencies show two regimes: (1) one with a sharp increase of η (regime I) and (2) another with a much slower increase of η (regime II). Current I_2 denotes the point where the regimes change. Quantitatively, we define I_2 as the current at which $\eta = 1\%$. The red dashed vertical lines denote I_2 for a 408-nm wavelength for each sample.

at $I > I_{\text{det}}^{\max}$ due to the small contribution of the near-edge region of the sample to full intrinsic detection efficiency. Therefore, we can safely assume that the current $I_2 \sim I_{\text{det}}^{\max}$.

The model of Ref. [8] predicts that the ratio $I_{\text{det}}^{\max}/I_{\text{dep}}$ increases at higher temperatures (see Fig. 11), and so does I_2/I_{dep}. This result qualitatively coincides with the present experimental findings. At $T = 4.2\ \text{K} \simeq 0.5T_c$, the ratio I_2/I_{dep} has a larger value for all of the bridges than at $T = 1.7\ \text{K} \simeq 0.2T_c$, but the deterministic regime extends over a wider current interval at lower temperatures. Moreover, for example, sample F ($w = 5.15\ \mu$m), with the lowest reduced critical current at $T = 4.2$ K, detects photons at high temperature only in the fluctuation-assisted regime, while at $T = 1.7$ K, it operates in the deterministic regime, too.

In our experiment, regime II extends over the current range of approximately $0.6I_{\text{dep}}$–$0.9I_{\text{dep}}$ (depending on the temperature and the specific sample), which is much wider than the theory [8] predicts. We also do not observe a saturation of η. We believe that the main reason is the geometry of our bridges, Fig. 1. The width of the bridge increases when one moves from its center to the leads and the local current density decreases. Therefore, with increasing current, a larger (longer) part of the bridge participates in the detection process and the η grows monotonically until the bridge switches to the resistive state at $I > I_c^{\text{sh}}$.

V. DISCUSSION

Now, we summarize and explain our observations by using the concept of vortex-assisted detection, introduced by Zotova and Vodolazov [7,8,15]. Because our samples have widths that are large compared to the estimated hot-spot diameter and to the coherence length, one expects that the detection mechanism should be insensitive to the width of the bridge, and dependent only on the supercurrent density j.

The model has one specific prediction. For a sufficiently large width of the bridge, the onset of deterministic detection is governed by the current density rather than by the current. Physically, this means that the registration of a detection event, which starts upon exceeding the critical current density (the critical supervelocity) [7,15], is sensitive only to the local density of the current (and to the size and "depth" of the spot, determined by the energy of the absorbed photon), but not to the distance between the hot spot and the edge of the strip. The latter requirement is true only if the strip is sufficiently wide compared to the size of the hot spot.

What "sufficiently wide" means is seen in Fig. 11, where the normalized detection current $I_{\text{det}}^{\max}/I_{\text{dep}}$, which is proportional to the density j_{det}, saturates near $w = 100\xi_c$. For simplicity of theoretical modeling, we use $\xi_c = \sqrt{\hbar D/k_B T_c}$ instead of the zero-temperature coherence length $\xi = \sqrt{\hbar D/\Delta(0)}$. For our bridges, $\xi_c = 5.4$ nm.

In our experiment, for most of the samples, $w > 100\xi_c$ holds, and we identify $I_{\text{det}}^{\max}$ with regime II with onset current I_2. Hence, the density of this current $I_2/w = j_{\text{det}}$ for a given wavelength is predicted to be the same for all of the samples (excluding perhaps the narrowest sample, A, with a width on the order of $100\xi_c$, which is a borderline case).

A direct check of this prediction needs to take into account the following two aspects: (1) there is some on-chip resistance in series with the superconducting bridge, and (2) there is the shunt resistance connected in parallel to the chip. Therefore, we do not know the current flowing *through the bridge* with sufficient accuracy. Hence, in the raw data in Fig. 6, one observes a spread of *measured* normalized detection currents I_2/I_{dep} over the different samples.

However, we note that the division of the current between the superconductor and the shunt being unknown varies from sample to sample; it is unaffected by the wavelength of the detected photons. This means that the ratio of the detection currents, *even those measured with a shunt*, corresponding to two wavelengths, $I_2(\lambda_1)/I_2(\lambda_2)$, should be the same for all samples with different widths. This prediction can be checked by renormalizing the bias current for all samples in a way which makes I_2—or, rather, I_2/w—the same for one wavelength. After this renormalization, we expect I_2/w at all other wavelengths to be the same for all samples.

Figure 7(a) demonstrates these results for a temperature of 1.7 K. We normalize the bias currents to match $\eta(I)$ at $\eta = 1\%$ for the wavelength of 408 nm. To relate the numbers to the current density, we apply the following procedure. We take the data for sample *B*, which has the closest values of critical current measured with and without a shunt and, hence, presumably the lowest on-chip serial resistance. We then calculate the current flowing through the superconducting bridge by multiplying the measured current to the ratio I_c/I_c^{sh} for this sample, and divide by I_{dep} at 1.7 K to obtain the ratio $j/j_{\mathrm{dep}} = I/I_{\mathrm{dep}}$. One can clearly observe that for the wavelength of 829 nm the detection current densities come very close to each other. This behavior holds also for wavelengths of 637 and 937 nm (not shown here). The only deviating sample is the narrowest sample, *A*, which is in line with the observations above.

For the largest wavelengths, 1310 (not shown) and 1550 nm, the spread of η curves at $\eta = 1\%$ between different samples is significantly larger, and it is problematic to state that they have the same detection current density after the normalization. We note, however, that, for these low energies of photons, the detection current by itself is not well defined because of the absence of a sharp increase of η above some current. We relate this effect to an increased role of fluctuations and local inhomogeneities with the decrease of energy deposited by the photon. Anyway, even for the largest wavelengths, the variation of j_{det} obtained after the normalization is still significantly less than the variation of I_2/w before this procedure.

The same argument about the dependence of η on j rather than on I holds also for fluctuation-assisted detection. In this case, one assumes that the detection events in this regime occur in the narrowest part of the bridge with the highest current density. This argument is also consistent with the data.

Next, for wide strips of constant width, the deterministic nature of detection should result in a steplike dependence of η in its dependence on j. $\eta \ll 100\%$ at $j < j_{\mathrm{det}}$, and $\eta = 100\%$ at $j > j_{\mathrm{det}}$. For our neck-shaped samples, we assume that we have unit probability of response to the absorbed photon in the central part of bridge, where $j > j_{\mathrm{det}}$. The probability is zero farther away from the narrowest part (see the inset in Fig. 7). The boundary between the inner and outer parts is set by the condition $j = j_{\mathrm{det}}$. Hence, introducing the area of the central, "detecting," part $S_{\mathrm{det}}(j)$, we derive the prediction that the internal detection efficiency is $\eta(j) = S_{\mathrm{det}}(j)/S$, where S is the total area of the bridge. [Details on the calculation of this $\eta(j)$ can be found in Appendix D]. Figure 7(b) compares this prediction with the experiment for wavelengths of 408 and 829 nm. One sees that the model reproduces three features: (i) a steeper increase of $\eta(j)$ for wider bridges, (ii) the convex shape of

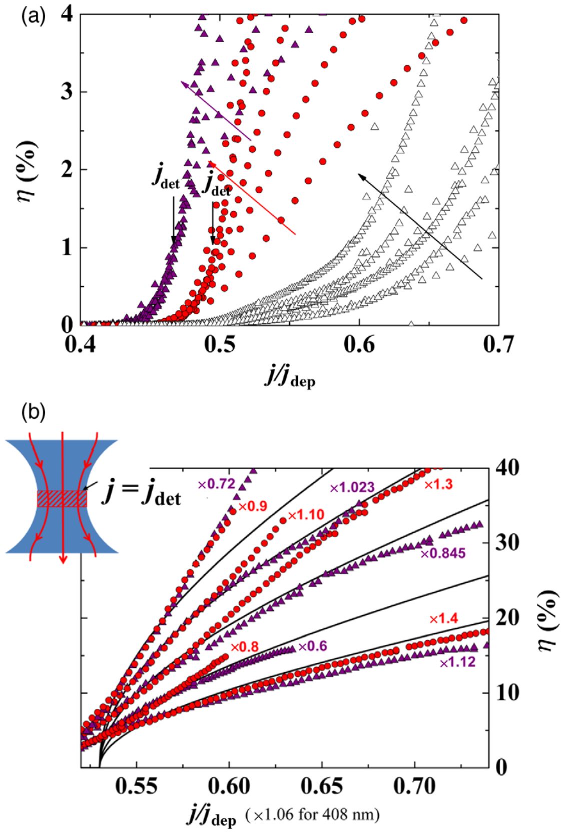

FIG. 7. (a) Dependencies of η on current density near the onset of regime II, demonstrating the invariance of the detection current density j_{det} with respect to the width of the bridge. Violet triangles, red circles, and empty black symbols correspond to the wavelengths of 408, 829, and 1550 nm. The widths of the samples are $w = 0.53$ μm (sample *A*), 1.06 and 1.61 μm (*B*), 2.12 μm (*C*), 3.07 μm (*D*), 4.07 μm (*E*), and 5.15 μm (*F*). Arrows show how they correspond to the curves, from narrow to wide. The temperature is 1.7 K. (b) η in regime II for wavelengths of 408 and 829 nm, compared to the ratio of the detecting area of the bridge to its total area. Data for samples *C*–*F* are shown, from bottom to top. The temperature is 1.7 K. (Inset) Schematics of bridge biased by a supercurrent. The part of the bridge at which $j > j_{\mathrm{det}}$ detects all absorbed photons, whereas the outer part with $j < j_{\mathrm{det}}$ does not.

the $\eta(j)$ dependencies, and (iii) up to a factor of 0.7–1.5, the absolute value of the measured η. The last discrepancy can be explained by the systematic and stochastic errors of our method of determining the η. The nonregular deviation of the curves for some of the samples from the model prediction can be attributed to defects in the samples. The model agrees with the experiment qualitatively, and even quantitatively for a sizable fraction of the samples. This is a strong indication that we observe photon detection with near-unity intrinsic probability at short wavelengths.

Comparing these findings to the predictions of the microscopic theory, we note that the observed detection current density $j_{\mathrm{det}} \approx 0.5 j_{\mathrm{dep}}$ for the wavelength of 408 nm is close to the calculated one [8]. As expected, j_{det} increases with the wavelength (i.e., with the decrease of photon energy) and appears to equal the experimental $j_c \approx 0.7 j_{\mathrm{dep}}$ for the wavelength of 1550 nm. This means that, to realize η close to unity for near-IR photons, one has to either reach a larger j_c/j_{dep} quantity or—an option which seems to be more achievable—enhance the effect of the hot spot, created by an IR photon, on the current density using thinner films.

VI. CONCLUSION

We develop in this paper single-photon detectors based on NbN microbridges. The dependence of the η on the supercurrent qualitatively resembles those of meander-type SSPDs with widths less than 200 nm. Our results demonstrate an alternative type of single-photon detector based on a short superconducting bridge with dimensions comparable to the diameter of an optical fiber and an η of about 1. This design provides a much shorter dead time, which is, in presently used detectors, several nanoseconds, due to the long length of the meander-type nanowire. Indirectly, our results confirm the vortex-assisted mechanism of photon detection using a wide current-carrying strip, as originally proposed by one of the authors [8].

ACKNOWLEDGMENTS

The work is supported by Russian Science Foundation (RSF) Project No. 17-72-30036. T. M. K. is also supported by European Research Council Advanced Grant No. 339306 (METIQUM).

APPENDIX A: DEVICE FABRICATION AND CHARACTERIZATION

The 5.8-nm-thick NbN film is deposited by dc magnetron sputtering of a niobium target in a plasma consisting of a mixture of argon (Ar) and nitrogen (N_2). The film is deposited on a silicon wafer with a buffer layer of silicon dioxide. The SiO_2 layer is 250 nm thick. Before starting the sputtering process, we heat the substrate to 400 °C. The film is characterized by a critical temperature of approximately $T_c = 8.3$ K. The deposition is done in the gas mixture with flow rates of 40 $\mathrm{cm^3\,min^{-1}}$ and 6.6 $\mathrm{cm^3\,min^{-1}}$ for Ar and N_2, respectively, and a current of 550 mA. The deposition rate under these conditions is 0.88 $\mathrm{Å\,s^{-1}}$.

The NbN film is patterned into a single bridge with rounded edges, using electron-beam lithography and the reactive ion etching technique. From one film, we make a batch of samples with different widths ranging from 0.53 to 5.15 μm. The size of each sample is determined with a SEM. All bridges are characterized by the critical temperature determined from the superconducting transition. The I-V curves are determined at temperatures of $T = 4.2$ K and $T = 1.7$ K. From a measurement of the temperature dependence of the second critical magnetic field, B_{c2} [Fig. 8(a)], we infer a diffusion constant D from the formula for diffusivity of the quasiparticles in the dirty superconductor [34]:

$$D = -\frac{4k_B}{\pi e}\left(\frac{dB_{c2}}{dT}\right)^{-1}. \tag{A1}$$

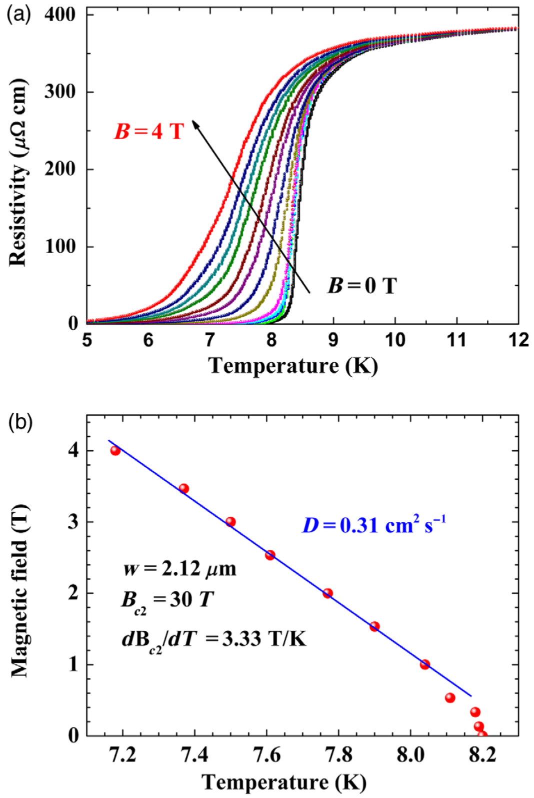

FIG. 8. (a) Dependence of resistivity on temperature for the 2.12-μm-wide sample C at different magnetic fields ranging from $B = 0$ T to $B = 4$ T. The black arrow indicates the direction of the increasing B values. (b) Measured temperature dependence of the critical magnetic field for the 2.12-μm-wide sample C (the circles), and linear fits of the data (the solid line) used for $B_{c2}(0)$ and the determination of the diffusivity.

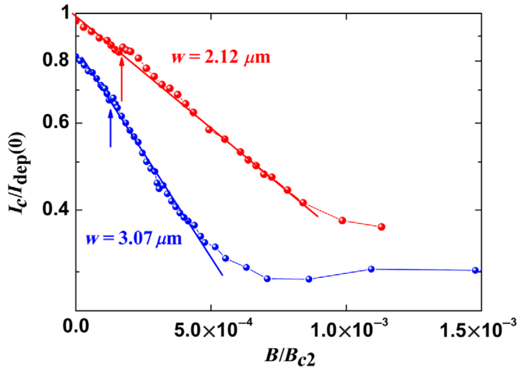

FIG. 9. Dependence of the normalized critical current $I_c/I_{\rm dep}(0)$ [I_c, critical current measured without the shunt; $I_{\rm dep}(0)$, theoretical depairing current at $T = 1.7$ K calculated from Eq. (2); $B_{c2}(1.7\text{ K}) = 23$ T] on the magnetic field measured for 2.12- and 3.07-μm-wide samples at a temperature $T = 1.7$ K. The linear dependence in low magnetic fields is evidence that the NbN film does not have large extrinsic defects leading to vortex pinning in the strip. The arrow-marked kinks are connected with the appearance of the single vortex chain in the middle of the bridge at that specific magnetic-field strength.

The calculated diffusivity is $D = 0.31\ \text{cm}^2\,\text{s}^{-1}$ [Fig. 8(b)]. This value is determined for one device and assumed to be identical for the other devices. Based on experiments on similar samples [35], we expect this assumption to cause an error of, at most, 20%. Extrapolating the linear temperature dependence of B_{c2} near T_c to $T = 0$, we find that $B_{c2}(0) = 30$ T.

As an additional proof of the high quality of our bridges, we measure the dependence of the critical current I_c on the perpendicular magnetic field B. Figure 9 shows the dependencies of I_c on B measured for devices C and D (2.12 and 3.07 μm wide). We find the linear decay $I_c(B)$ at low magnetic fields, which demonstrates the dominant contribution of the edge barrier for vortex entry [36] and kinks in the dependence of $I_c(B)$ at $B/B_{c2} \approx 10^{-3}$ (marked by arrows), which are connected to the presence of the single vortex chain in the middle of the bridge [14,37,38]. Neither of these results can be observed in the bridge with a dominant contribution of bulk pinning to I_c and the presence of a large number of defects able to pin the vortices.

APPENDIX B: EXPERIMENTAL SETUP AND MEASUREMENTS

The electro-optical characterization of our samples is performed in a fiber-based setup. The sample is mounted on a dipstick to be inserted into a liquid He Dewar. The measurements are carried out at two temperatures: $T = 4.2$ K and $T = 1.7$ K. The latter is reached by vacuum pumping the helium from a cryoinsert for a storage Dewar. As light sources, we use light-emitting diodes with wavelengths of 408, 637, 829, 937, 1330, and 1550 nm which can be operated in both pulsed and cw regimes. The sample chip with the transmission line is connected to a dc + rf–output port of a bias tee. The bias current is supplied through the dc port. We connect a 3-Ω resistor in parallel to the sample to prevent latching when the critical current is exceeded. The voltage pulse is amplified by two room-temperature Mini-Circuits ZFL-1000LN+ (1-GHz band, 46-dB total gain) amplifiers, and it is fed to a digital oscilloscope and a pulse counter [Agilent 53131A (225-MHz band)].

In view of the topology and the small active area of our samples, we do not package them with a single-mode fiber, as is usually done with meander SSPDs [39,40]. For the present measurements, we use the sample holder shown in Fig. 10. In this sample holder, we use the optical fiber SM-28, which is single mode for wavelength 1550 nm, with a 9-μm core diameter and a $\mathcal{N}$ (numerical aperture) of 0.14. However, at lower cutoff wavelengths (below 1260 nm), the mode distribution in SM-28 fiber is not Gaussian because the fiber becomes multimodal [41]. To illuminate our bridge uniformly, we increase the diameter of the output Gaussian beam by placing the sample at a distance of $d = 80$ mm from the end of the fiber. Figure 10 shows the calculated field profiles emitted from the fiber for

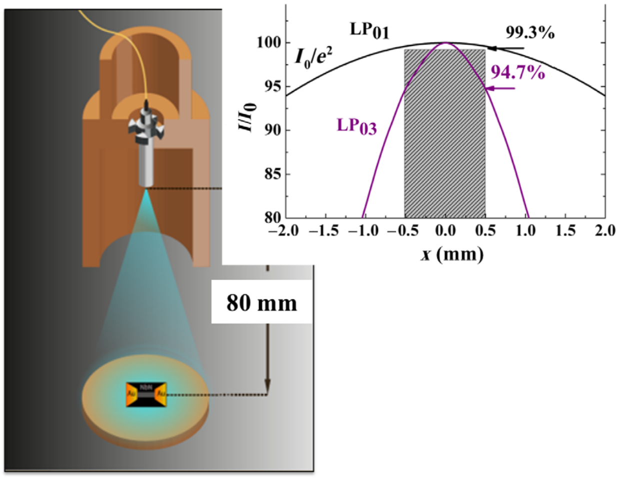

FIG. 10. A sketch of the sample illumination principle: to produce a uniform illumination with a relatively large area, we place the sample 80 mm away from the fiber pigtail. (Inset) Calculation of the light-beam intensity profile at the sample plane. Curve LP_{01} is a single-mode profile which is observed in SM-28 fiber for wavelengths longer than 1 μm. It is a Gaussian profile calculated as $I = I_0 \exp(2x^2/r_0{}^2)$, with I_0 being the irradiance at the center of the beam and r_0 the radius of the beam at which the irradiance is I_0/e^2 and $r_0 = d\mathcal{N}$, where d is the distance from the surface of the optical fiber to the surface of the detector and $\mathcal{N}$ is the numerical aperture. For fiber SM-28, $r_0 = 11.2$ mm. Curve LP_{03} corresponds to the multimode profile at 408-nm wavelength, and it is described by Bessel functions of the second kind. The gray rectangle corresponds to a 0.5-mm displacement. One can see that, in the worst case, the light intensity is at least 94% of its maximum in the center.

the wavelengths 1500 and 408 nm. At wavelengths of 1310 and 1550 nm, the light intensity within a 1-mm-diameter spot is not less than 99% of the light intensity in the center (the LP_{01} profile shown in Fig. 10). For the 408-nm wavelength, the mode profile is narrower (LP_{03} in Fig. 10), but, even in this case, if the device is displaced by ±0.5 mm, the light intensity is not less than 95% of the intensity in the center.

The dipstick is calibrated with a meander SSPD with a filling factor of 50% (100-nm strip and 100-nm gap). The η of the meander SSPD has been previously measured by packaging it with single-mode fibers. Subsequent measurements of this sample in the dipstick with a known detection efficiency make it possible to determine the number of photons in the flow incident on the sample with an area of 10×10 μm. Knowing the ratio of the areas of the meander-shaped SSPD and the bridge, we calculate the number of photons incident on the bridge.

APPENDIX C: THEORETICAL ESTIMATES

In Fig. 11, we present the calculated dependence of $I_{\mathrm{det}}^{\max}/I_{\mathrm{dep}}$ on the temperature for strips with different widths and two wavelengths. The results are obtained in the framework of the two-temperature hot-spot model developed by one of the authors in Ref. [8]. The calculations are carried out at temperatures of $T \geq 0.35T_c$, where the numerical procedure converges well. In this model, $I_{\mathrm{det}}^{\max}$ is defined as the maximal value of the detection current at which all points across the strip participate in the photon detection (and where the intrinsic detection efficiency reaches unity). The growth of $I_{\mathrm{det}}^{\max}/I_{\mathrm{dep}}$ with temperatures ranging from $0.35T_c$ to $0.7T_c$ is connected to the nonlinear temperature dependence of the electronic and phonon energies [8]. The growth of $I_{\mathrm{det}}^{\max}/I_{\mathrm{dep}}$ at a temperature $T \gtrsim 0.7T_c$ for wide strips ($w > 40\xi_c$ and $\xi_c = 5.4$ nm for our bridges, as shown above) is explained by the rapid drop of $I_{\mathrm{dep}}(T)$. This leads to a reduced Joule heating in the superconductor when the first vortex-antivortex pair nucleates inside the (nonequilibrium) hot spot and worsens conditions for the appearance of a fully normal domain. This is the case for the same reason that $I_{\mathrm{det}}^{\max}/I_{\mathrm{dep}}$ grows for a strip with $w = 20\xi_c$ and $\lambda = 620$ nm at $T > 0.85T_c$. One would expect that, with the approach to T_c, photon detection becomes impossible [8] because the normal domain cannot appear in the strip.

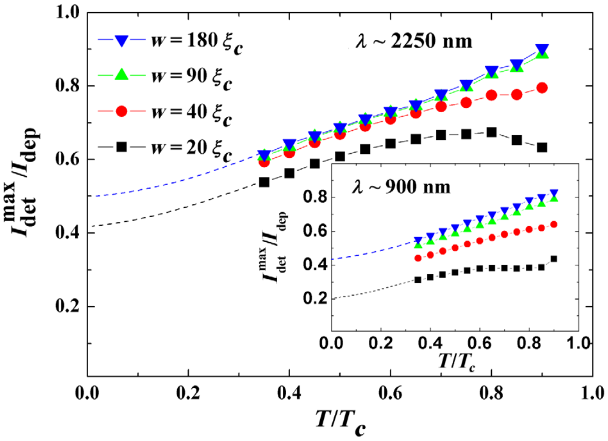

FIG. 11. Dependence of $I_{\mathrm{det}}^{\max}/I_{\mathrm{dep}}$ on temperature for two wavelengths, $\lambda = 2250$ nm and $\lambda = 900$ nm (inset), of the photon and at different widths of the strip. At the current $I \geq I_{\mathrm{det}}^{\max}$, all points across the strip participate in photon detection, and the intrinsic detection efficiency reaches unity. Calculations are made in the framework of the $2T$ hot-spot model in Ref. [8]. Dashed lines show the expected dependence at low temperatures (they follow from results using the hot-belt model—see Fig. 6 in Ref. [8]), where the numerical scheme from Ref. [8] does not converge.

In the calculations, we assume that the escape time of the nonequilibrium phonons to the substrate, τ_{esc}, is equal to the characteristic time $\tau_0 \sim 270$ ps and, furthermore, that the important parameter $\gamma = 10$. Both are typical values for NbN (for the definition of τ_0 and γ, see Ref. [8]). Choosing a smaller value of τ_{esc} (up to $0.1\tau_0$) hardly changes the obtained dependencies, at least for temperatures $T < 0.8T_c$, because the time for the nucleation of a normal domain δt [8] does not exceed $0.1\tau_0$. At $T = 0.9T_c$, the time δt approaches $0.4\tau_0$ for a strip with $w = 180\xi_c$. A smaller value of τ_{esc} provides a large value of $I_{\mathrm{det}}^{\max}/I_{\mathrm{dep}}$.

APPENDIX D: ACCOUNTING FOR THE NONRECTANGULAR SHAPE OF THE BRIDGES

To apply our simple model of deterministic detection, which predicts $\eta = 0$ at $j < j_{\mathrm{det}}$ and $\eta = 1$ at $j > j_{\mathrm{det}}$, to our bridges with nonconstant widths, and hence nonconstant j values over the length, we calculate the detecting amount of the bridge area, in which $j > j_{\mathrm{det}}$. To do so, we introduce coordinates as shown in Fig. 12. We express the area of the bridge segment of length $2x$ as

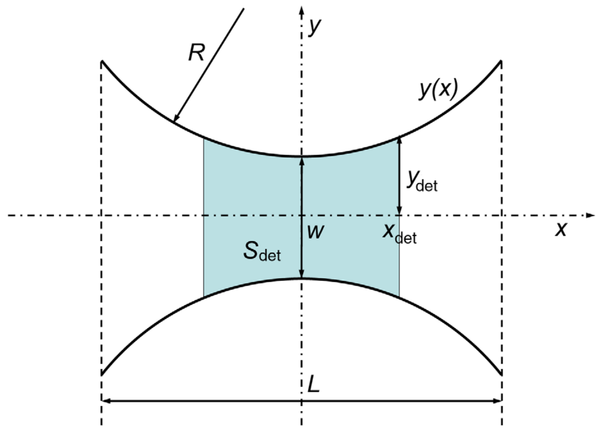

FIG. 12. Calculation of the detecting area S_{det}.

$S(x) = 4\int y(x)dx \approx 2wx + 2x^3/3R$, where $y(x) = w/2 + R - \sqrt{R^2 - x^2} \approx w/2 + x^2/2R$ is the half width of the bridge at the cross section with the coordinate x. The current density at the same cross section is $j(x) = jw/y(x)$, with j being the current density at the center of the bridge, $x = 0$. At the boundary between the detecting and nondetecting parts, $x_{\rm det}$, one has $j(x_{\rm det}) = j_{\rm det}$ and $y(x_{\rm det}) = (j/j_{\rm det})(w/2)$. Expressing the half width at this boundary as $y_{\rm det} \approx Rw\sqrt{j/j_{\rm det} - 1}$, we derive that the detecting area $S_{\rm det}=S(x_{\rm det})\approx R^{1/2}w^{3/2}[2(j/j_{\rm det}-1)^{1/2}+(2/3)(j/j_{\rm det}-1)^{3/2}]$. Finally, to obtain $\eta(j) = S_{\rm det}/S$, we divide $S_{\rm det}(j)$ by the total area of bridge, $S \approx wL + L^3/12R$.

[1] C. M. Natarajan, M. G. Tanner, and R. H. Hadfield, Superconducting nanowire single-photon detectors: Physics and applications, Supercond. Sci. Technol. **25**, 063001 (2012).
[2] L. Maingault, M. Tarkhov, I. Florya, A. Semenov, R. Espiau de Lamaëstre, P. Cavalier, G. Goltsman, J.-P. Poizat, and J.-C. Villégier, Spectral dependency of superconducting single photon detectors, J. Appl. Phys. **107**, 116103 (2010).
[3] R. Lusche, A. Semenov, K. Ilin, M. Siegel, Y. Korneeva, A. Trifonov, A. Korneev, G. Gol'tsman, D. Vodolazov, and H.-W. Hübers, Effect of the wire width on the intrinsic detection efficiency of superconducting-nanowire single-photon detectors, J. Appl. Phys. **116**, 043906 (2014).
[4] A. Semenov, G. Gol'tsman, and A. Korneev, Quantum detection by current carrying superconducting film, Physica (Amsterdam) **351C**, 349 (2001).
[5] A. Semenov, A. Engel, H.-W. Hübers, K. Il'in, and M. Siegel, Spectral cut-off in the efficiency of the resistive state formation caused by absorption of a single-photon in current-carrying superconducting nano-strips, Eur. Phys. J. B **47**, 495 (2005).
[6] Wordenweber Roger, Moshchalkov Victor, Bending Simon, and Tafuri Francesco, *Superconductors at the Nanoscale* (Walter de Gruyter GmbH, Berlin, 2017).
[7] A. N. Zotova and D. Y. Vodolazov, Photon detection by current-carrying superconducting film: A time-dependent Ginzburg-Landau approach, Phys. Rev. B **85**, 024509 (2012).
[8] D. Yu. Vodolazov, Single-Photon Detection by a Dirty Current-Carrying Superconducting Strip Based on the Kinetic-Equation Approach, Phys. Rev. Applied **7**, 034014 (2017).
[9] A. Kamlapure, M. Mondal, M. Chand, A. Mishra, J. Jesudasan, V. Bagwe, L. Benfatto, V. Tripathi, and P. Raychaudhuri, Measurement of magnetic penetration depth and superconducting energy gap in very thin epitaxial NbN films, Appl. Phys. Lett. **96**, 072509 (2010).
[10] A. Kamlapure, T. Das, S. C. Ganguli, J. B. Parmar, S. Bhattacharyya, and P. Raychaudhuri, Emergence of nanoscale inhomogeneity in the superconducting state of a homogeneously disordered conventional superconductor, Sci. Rep. **3**, 2979 (2013).
[11] H. L. Hortensius, E. F. C. Driessen, and T. M. Klapwijk, Possible indications of electronic inhomogeneities in superconducting nanowire detectors, IEEE Trans. Appl. Supercond. **23**, 2200705 (2013).
[12] J. Romijn, T. M. Klapwijk, M. J. Renne, and J. E. Mooij, Critical pair-breaking current in superconducting aluminum strips far below T_c, Phys. Rev. B **26**, 3648 (1982).
[13] I. Charaev, T. Silbernagel, B. Bachowsky, A. Kuzmin, S. Doerner, K. Ilin, A. Semenov, D. Roditchev, D. Yu. Vodolazov, and M. Siegel, Proximity effect model of ultranarrow NbN strips, Phys. Rev. B **96**, 184517 (2017).
[14] K. Ilin, D. Henrich, Y. Luck, Y. Liang, M. Siegel, and D. Yu. Vodolazov, Critical current of Nb, NbN, and TaN thin-film bridges with and without geometrical nonuniformities in a magnetic field, Phys. Rev. B **89**, 184511 (2014).
[15] A. Zotova and D. Y. Vodolazov, Intrinsic detection efficiency of superconducting nanowire single photon detector in the modified hot spot model, Supercond. Sci. Technol. **27**, 125001 (2014).
[16] J. R. Clem and K. K. Berggren, Geometry-dependent critical currents in superconducting nanocircuits, Phys. Rev. B **84**, 174510 (2011).
[17] L. G. Aslamazov and A. I. Larkin, Josephson effect in superconducting point contacts, JETP Lett. **9**, 87 (1969), http://www.jetpletters.ac.ru/ps/1658/article_25296.shtml.
[18] K. K. Likharev, Superconducting weak links, Rev. Mod. Phys. **51**, 101 (1979).
[19] M. W. Brenner, D. Roy, N. Shah, and A. Bezryadin, Dynamics of superconducting nanowires shunted with an external resistor, Phys. Rev. B **85**, 224507 (2012).
[20] J. Bardeen, Critical fields and currents in superconductors, Rev. Mod. Phys. **34**, 667 (1962).
[21] J. R. Clem and V. G. Kogan, Kinetic impedance and depairing in thin and narrow superconducting films, Phys. Rev. B **86**, 174521 (2012).
[22] Z. Wang, A. Kawakami, Y. Uzawa, and B. Komiyama, Superconducting properties and crystal structures of single-crystal niobium nitride thin films deposited at ambient substrate temperature, J. Appl. Phys. **79**, 7837 (1996).
[23] S. P. Chockalingam, M. Chand, A. Kamlapure, J. Jesudasan, A. Mishra, V. Tripathi, and P. Raychaudhuri, Optical and transport properties of ultrathin NbN films and nanostructures, Phys. Rev. B **79**, 094509 (2009).
[24] M. Beck, M. Klammer, S. Lang, P. Leiderer, V. V. Kabanov, G. N. Goltsman, and J. Demsar, Energy-Gap Dynamics of Superconducting NbN Thin Films Studied by Time-Resolved Terahertz Spectroscopy, Phys. Rev. Lett. **107**, 177007 (2011).
[25] Y. Noat, V. Cherkez, C. Brun, T. Cren, C. Carbillet, F. Debontridder, K. Ilin, M. Siegel, A. Semenov, H.-W. Hübers, and D. Roditchev, Unconventional superconductivity in ultrathin superconducting NbN films studied by scanning tunneling spectroscopy, Phys. Rev. B **88**, 014503 (2013).
[26] R. Romestain, B. Delaet, P. Renaud-Goud, I. Wang, J.-C. Villegier, C. Jorel, and J.-Ph. Poizat, Fabrication of a superconducting niobium nitride hot electron bolometer for single-photon counting, New J. Phys. **6**, 129 (2004).
[27] B. Spivak, A. Kapitulnik, and S. A. Kivelson, Anomalous metals—Failed superconductors, arXiv:1712.07215.

[28] A. Semenov, B. Günther, U. Böttger, H.-W. Hübers, H. Bartolf, A. Engel, A. Schilling, K. Ilin, M. Siegel, R. Schneider, D. Gerthsen, and N. A. Gippius, Optical and transport properties of ultrathin NbN films and nanostructures, Phys. Rev. B **80**, 054510 (2009).

[29] A. Kerman, E. Dauler, W. Keicher, J. Yang, K. Berggren, G. Gol'tsman, and B. Voronov, Kinetic-inductance-limited reset time of superconducting nanowire photon counters, Appl. Phys. Lett. **88**, 111116 (2006).

[30] G. Gol'tsman, O. Okunev, G. Chulkova, A. Lipatov, A. Semenov, K. Smirnov, B. Voronov, A. Dzardanov, C. Williams, and R. Sobolewski, Picosecond superconducting single-photon optical detector, Appl. Phys. Lett. **79**, 705 (2001).

[31] Yu. Korneeva, I. Florya, S. Vdovichev, M. Moshkova, N. Simonov, N. Kaurova, A. Korneev, and G. Goltsman, Comparison of hot spot formation in NbN and MoN thin superconducting films after photon absorption, IEEE Trans. Appl. Supercond. **27**, 2201504 (2017).

[32] F. Marsili, F. Najafi, E. Dauler, F. Bellei, M. Csete, X. Hu, R. J. Molnar, and K. K. Berggren, Single-photon detectors based on ultranarrow superconducting nanowires, Nano Lett. **11**, 2048 (2011).

[33] A. Engel, J. Lonsky, X. Zhang, and A. Schilling, Detection mechanism in SNSPD: Numerical results of a conceptually simple, yet powerful detection model, IEEE Trans. Appl. Supercond. **25**, 2200407 (2015).

[34] Holger Bartolf, *Fluctuation Mechanisms in Superconductors* (Springer Spektrum, Wiesbaden, Germany, 2016).

[35] M. Shcherbatenko, I. Tretyakov, Yu. Lobanov, S. N. Maslennikov, N. Kaurova, M. Finkel, B. Voronov, G. Goltsman, and T. M. Klapwijk, Nonequilibrium interpretation of dc properties of NbN superconducting hot electron bolometers, Appl. Phys. Lett. **109**, 132602 (2016).

[36] B. L. T. Plourde, D. J. Van Harlingen, D. Y. Vodolazov, R. Besseling, M. B. S. Hesselberth, and P. H. Kes, Influence of edge barriers on vortex dynamics in thin weak-pinning superconducting strips, Phys. Rev. B **64**, 014503 (2001).

[37] V. V. Shmidt, The critical current in superconducting films, Sov. Phys. JETP **30**, 1137 (1970), http://jetp.ac.ru/cgi-bin/dn/e_030_06_1137.pdf.

[38] D. Y. Vodolazov, Vortex-induced negative magnetoresistance and peak effect in narrow superconducting films, Phys. Rev. B **88**, 014525 (2013).

[39] S. Miki, M. Fujiwara, M. Sasaki, and Z. Wang, NbN superconducting single-photon detectors prepared on single-crystal MgO substrates, IEEE Trans. Appl. Supercond. **17**, 285 (2007).

[40] W. Slysz *et al.*, Fiber-coupled single-photon detectors based on NbN superconducting nanostructures for practical quantum cryptography and photon-correlation studies, Appl. Phys. Lett. **88**, 261113 (2006).

[41] John M. Senior and M. Yousif Jamro, *Optical Fiber Communications: Principles and Practice* (Ashford Colour Press, Gosport, England, 2009).